Multi-material topology optimization of viscoelastically damped structures using a parametric level set method

van der Kolk, Max; van der Veen, Gijs; de Vreugd, J; Langelaar, Matthijs

DOI
10.1177/1077546315617333

Publication date
2017

Document Version
Final published version

Published in
Journal of Vibration and Control

Citation (APA)
van der Kolk, M., van der Veen, G., de Vreugd, J., & Langelaar, M. (2017). Multi-material topology optimization of viscoelastically damped structures using a parametric level set method. *Journal of Vibration and Control*, *23*(15), 2430-2443. https://doi.org/10.1177/1077546315617333

Article

Journal of Vibration and Control
2017, Vol. 23(15) 2430–2443

DOI: 10.1177/1077546315617333
journals.sagepub.com/home/jvc
SAGE

Multi-material topology optimization of viscoelastically damped structures using a parametric level set method

Max van der Kolk[1,2], Gijs J van der Veen[1], Jan de Vreugd[2] and Matthijs Langelaar[1]

Abstract

The design of high performance instruments often involves the attenuation of poorly damped resonant modes. Current design practices typically rely on informed trial and error based modifications to improve dynamic performance. In this article, a multi-material topology optimization approach is presented as a systematic methodology to develop structures with optimal damping characteristics. The proposed method applies a multi-material, parametric, level set-based topology optimization to simultaneously distribute structural and viscoelastic material to optimize damping characteristics. The viscoelastic behavior is represented by a complex-valued material modulus resulting in a complex-valued eigenvalue problem. The structural loss factor is used as objective function during the optimization and is calculated using the complex-valued eigenmodes. An adjoint sensitivity analysis is presented that provides an analytical expression for the corresponding sensitivities. Multiple numerical examples are treated to illustrate the effectiveness of the approach and the influence of different viscoelastic material models on the optimized designs is studied. The optimization routine is able to generate designs for a number of eigenmodes and to attenuate a resonant mode of an existing structure.

Keywords

Viscoelastic damping, topology optimization, multi-material optimization, level set method, loss factor, modal analysis, constrained layer damping

1. Introduction

This paper addresses the design of structures composed of both viscoelastic and structural material, to achieve optimal damping characteristics. This is implemented using a multi-material level set-based topology optimization. The design of high-performance instruments often involves the attenuation of poorly damped resonant modes. At the Netherlands Organisation for Applied Scientific Research (TNO) this is encountered during the design of high performance optomechatronic instruments (De Vreugd et al., 2014), such as GAIA BAM (Gielesen et al., 2013) and MSI VNS (Tabak et al., 2013). Current design approaches typically start from a baseline design and introduce stiffening or damping reinforcements to tune and damp these modes. However, the influence of these reinforcements is difficult to predict, resulting in a trial and error approach. We propose an integrated multi-material topology optimization approach as a systematic methodology for the development of these structures. Designs involving multiple appropriately distributed materials, in particular the combination with viscoelastic materials, are known to provide high structural damping and have been applied in many fields (Johnson, 1995), for example in automotive and aviation (Rao, 2003), aerospace (Rittweger et al., 2002; Wang et al., 2008), and civil applications (Samali and Kwok, 1995; Wang et al., 2013).

[1]Department of Precision and Microsystems Engineering, Delft University of Technology, The Netherlands
[2]Optomechatronics, Netherlands Organisation for Applied Scientific Research, The Netherlands

Received: 10 June 2015; accepted: 21 October 2015

Corresponding author:
Max van der Kolk, Department of Precision and Microsystems Engineering, Delft University of Technology, Mekelweg 2, 2628 CD Delft, The Netherlands.
Email: M.vanderKolk@tudelft.nl

Viscoelastic materials dissipate energy when subjected to deformation. To achieve optimal damping the viscoelastic material has to be placed at locations which undergo large deformation during vibration. Besides, the design of the construction itself should promote deformation of the viscoelastic material. The two most common damping geometries for viscoelastic dampers are unconstrained and constrained layer damping (Grootenhuis, 1970). Here, the viscoelastic material is constrained on one or both sides. During vibration the viscoelastic material is forced to deform and thereby dissipate energy.

The development of viscoelastic dampers presents a challenging optimization problem, where the goal is to achieve optimal structural damping. Both the location as well as the geometry of the viscoelastic layer can be determined using an optimization routine. In previous studies both analyses have been performed separately, for example, the placement of viscoelastic patches along a vibrating frame (Lunden, 1980) and the shape optimization of individual, unconstrained and constrained viscoelastic layers (Lumsdaine and Scott, 1998; Plunkett and Lee, 1970). The loss factor (Kerwin, 1959) is determined for each structure to quantitatively compare the amount of structural damping for each design.

More recent studies have applied topology optimization to find optimized damping characteristics by distribution of viscoelastic material in the design domain. The optimization method searches for the distribution of viscoelastic material to obtain the highest loss factors for single or multiple modeshapes. These optimization routines are implemented for unconstrained layer damping on plates (El-Sabbagh and Baz, 2013) and shell structures under harmonic excitations (Kang et al., 2012). Here, an additional layer of viscoelastic material is optimally distributed on top of the plates to dissipate energy during vibrations. Similar approaches are available for constrained layer treatments: for simply supported beams (Zheng et al., 2004) and vibrating plates (Ling et al., 2011; Zheng et al., 2013). In these designs the viscoelastic layer is sandwiched by two beams or plates and its distribution within this layer is optimized. However, these optimization routines limit the design domain of viscoelastic material to the predefined (un)constrained layer. Before the optimization, the location of the viscoelastic layer is to be provided by the designer.

Multiple modeling approaches have been presented to model the viscoelastic behavior. The material can be represented using models based on springs and dashpots, for example, the Maxwell or Kevin-Voigt models (Bert, 1973) and extensions hereof. Alternatively, the elastic and dissipative behavior can be represented by a complex material modulus (Grootenhuis, 1970). For the modeling of harmonically excited structures, this latter method is widely applied, for example, by Kerwin (1959) and Johnson (1995) and the previously mentioned optimization routines. The studies apply different formulations of the complex modulus. For example, the authors of Lunden (1980), Rao (1978) and El-Sabbagh and Baz (2013) apply a complex Young's modulus, while the authors Liu et al. (2013) and Ling et al. (2011) only apply a complex shear modulus. When the complex modulus is limited to the shear modulus, only deformations with shear components dissipate energy. For the analysis of beams or plates using constrained layer configurations, the difference between using a complex Young's or shear modulus might not result in significant performance changes; the obtained modeshapes show predominately shear deformation within the viscoelastic layer. Yet, when optimizing arbitrary geometries the choice of complex modulus might steer the optimization towards specific designs. In this paper we devote specific attention to this point.

The implementation of the complex material modulus provides a complex-valued stiffness matrix, resulting in a complex-valued eigenvalue problem to determine the structure's natural modes. In the mentioned studies, a number of approximations are made regarding the calculation of the loss factor and its sensitivities. In some papers the loss factors are calculated using the eigenmodes obtained from the undamped analysis (Kim, 2011; Liu et al., 2013; Ling et al., 2011; Zheng et al., 2013). However, for low structural damping, we have observed that the eigenmodes of the undamped and damped structure are approximately the same. At higher structural damping it will be required to move towards the complex modeshapes for the calculations. Similarly, it is observed that the sensitivities of the loss factor are determined using approximations. For example, by neglecting the contribution of the modeshape sensitivity to changes in the design (Ling et al., 2011), or by using an approximate formulation (Wang et al., 2014; Zheng et al., 2013).

Several multi-material topology optimization routines are available for various optimization methods, such as, the density methods by Sigmund (2001) and Yin and Ananthasuresh (2001), the evolutionary implementation by Huang and Xie (2009) and the level set methods by Wang and Wang (2004) and Allaire et al. (2014). For multi-material or multi-phase optimization, the level set method has the advantage of distinct separation between the different materials. To overcome numerical difficulties from tracking the boundaries and solving the Hamilton–Jacobi convection equations, the level set functions have been parameterized (Luo et al., 2007; Wang and Wang, 2006). The parametric level set methods describe the level set function by a set of shape functions and expansion coefficients, while

maintaining distinct separation between material phases. A recent overview of the level set methods and parametrization approaches is given in Van Dijk et al. (2013). The parametric level set methods have recently been extended towards multi-material optimization (Wang et al., 2015).

In this article a multi-material topology optimization formulation is developed. Here, the viscoelastic and structural material will be distributed simultaneously to achieve optimal damping characteristics. Within the user-specified bounds the obtained designs can have arbitrary material distributions and geometries, possibly resulting in higher levels of structural damping. Also, there is no need to predefine a location of the viscoelastic layer by the designer. Furthermore, the calculation of the loss factors is performed using the complex-valued modeshapes and an exact formulation is proposed for the loss factor sensitivities.

The article is organized as follows. Section 2 describes the modeling of the viscoelastic material and investigates the obtained loss factor definitions for a constrained layer configuration. Then, Section 3 provides the formulation of the parametric, multi-material level set method, the objective and constraints, and the adjoint sensitivity analysis. In Section 4 the results of two case studies are presented and discussed. The paper ends with conclusions regarding the proposed optimization routine.

2. Modeling of viscoelastic material

In this paper the viscoelastic material is described using a complex material modulus. The formulation of the material model is discussed in the following sections. Furthermore, the structural loss factor is introduced as a measure to compare the structural damping between different structures. Different methods to calculate the loss factor are shown and their performance to represent the structural damping for viscoelastically damped structures are compared.

2.1. Complex material modulus

When a viscoelastic material is deformed dynamically the corresponding stresses are not in phase with the applied strains (Tschoegl, 1989). For a harmonically excited structure the stress will lead the applied strain by an angle θ. The strain ε and stress σ are represented as

$$\begin{aligned} \varepsilon(t) &= \varepsilon_0 \sin(\omega t) \\ \sigma(t) &= \sigma_0(\omega) \sin(\omega t + \theta(\omega)) \end{aligned} \tag{1}$$

For harmonically excited structures the observed phase angle can be represented by applying a complex material modulus. The complex material modulus is found by dividing the stresses by the strains (Grootenhuis, 1970; Tschoegl, 1989). This results in

$$E(\omega) = E(\omega)' + iE(\omega)'' \tag{2}$$

The Young's modulus is given by a complex quantity, with i being the complex number $i = \sqrt{-1}$. The material modulus is given by the storage modulus E' and the loss modulus E''. These components are responsible for the elastic and dissipative behavior, respectively. Many different models are available to describe the viscoelastic behavior. The complex material model is applied for its relative simplicity and ease of modeling responses of viscoelastic structures to harmonic excitations. For a general viscoelastic material the moduli depend on both temperature and excitation frequency. In the presented work the material moduli are assumed constant to simplify the material description. The storage and loss modulus are related through the material loss factor η and the loss angle θ

$$\frac{E''}{E'} = \tan(\theta) = \eta \tag{3}$$

A similar approach can be applied to define a complex bulk (κ) or shear (G) modulus. Depending on the applied viscoelastic material any complex modulus can be chosen to represent the dissipative behavior

$$\begin{aligned} E &= E'(1 + i\eta) \\ \kappa &= \kappa'(1 + i\eta) \\ G &= G'(1 + i\eta) \end{aligned} \tag{4}$$

When a complex bulk or shear modulus is applied, the viscoelastic material only dissipates energy when the deformation contains the corresponding bulk or shear components. However, when a complex Young's modulus is applied the viscoelastic material will dissipate energy for any deformation.

The behavior of the continuum body with a structural and viscoelastic material is described by the following equilibrium condition

$$\begin{cases} \operatorname{div}(C_\chi \varepsilon(u)) + f - \rho_\chi \ddot{u} = 0 & \text{in } D \\ u = 0 & \text{on } \Gamma_D^k \end{cases} \tag{5}$$

The constitutive constant is scaled using a Voigt mixing law and is based on the presence of the material phases k: $C_\chi = C^k \chi^k$, where χ^k is a function of phase Ω^k. A similar scaling is applied for the material density ρ_χ. The applied body forces are given by f, the displacement by u and the strains by ε. To account for the phase lag between stresses and strains the elastic coefficients with C_χ can take on complex values. For the remaining

analysis the system is discretized in finite elements providing the following discretized equations of motion. Due to the application of complex-valued elastic coefficients the stiffness matrix is complex-valued

$$\boldsymbol{M}\ddot{\boldsymbol{x}} + (\boldsymbol{K}_{\mathrm{R}} + i\boldsymbol{K}_{\mathrm{I}})\boldsymbol{x} = \boldsymbol{f} \tag{6}$$

with $\boldsymbol{M}$ the global mass matrix, $\boldsymbol{K}_{\mathrm{R}}$ and $\boldsymbol{K}_{\mathrm{I}}$ respectively the real and imaginary parts of the global stiffness matrix, $\boldsymbol{x}$ the nodal displacements and $\boldsymbol{f}$ the forces applied to the structure. The imaginary components of the stiffness matrix model the dissipative behavior.

The applied viscoelastic material model also results in a complex eigenvalue problem

$$\left(-\lambda^2\boldsymbol{M} + (\boldsymbol{K}_{\mathrm{R}} + i\boldsymbol{K}_{\mathrm{I}})\right)\phi = \boldsymbol{0} \tag{7}$$

The obtained eigenfrequencies λ and eigenmodes ϕ are therefore complex-valued.

The harmonically excited, viscoelastic structures show a steady-state oscillatory deformation. Part of the excitation energy is stored elastically, while the remainder is dissipated within the viscoelastic material. In a stress-strain diagram, this dissipative oscillation results in a hysteresis loop. The dissipated energy per unit volume during each cycle is determined from the contour integral along the hysteresis loop. The hysteresis loop is constructed by plotting the stress $\sigma(t)$ as a function of the strain $\varepsilon(t)$. The dissipated energy per unit volume for a cycle W_{cyc} has been derived by Tschoegl (1989). It has to be noted that this derivation can be performed for either choice of complex material modulus. To illustrate the obtained expressions, the derivation has been performed with a complex shear modulus, resulting in the following expressions for the dissipated energy

$$W_{\mathrm{cyc}} = \oint \sigma(t)\varepsilon(t) = \pi\varepsilon_0^2 G'' \tag{8}$$

By multiplication with the corresponding excitation frequency the dissipated power per unit volume is found. Since the eigenfrequencies are given in rad/s the result is divided by 2π to obtain power

$$Q_{\mathrm{dissip}} = \frac{1}{2}\lambda\varepsilon_0^2 G'' \tag{9}$$

With the complex material modulus, the dissipated energy can also be determined from the imaginary part of the stiffness matrix in combination with a modeshape corresponding to the deformation. Then, the dissipated energy per cycle is given as

$$W_{\mathrm{cyc}} = \pi\phi^{\mathrm{H}}\boldsymbol{K}_{\mathrm{I}}\phi \tag{10}$$

The superscript ϕ^{H} indicates the conjugate transpose.

2.2. Structural loss factor

To quantitively compare the damping between different structures the structural loss factors are determined. A general formulation of the structural loss factor has been proposed by Johnson and Kienholz (1982). The structural loss factor describes the ratio between dissipated and stored energy. The structural loss factor for eigenmode r is given by

$$\bar{\gamma}_r = \frac{\boldsymbol{\psi}_r^T\boldsymbol{K}_{\mathrm{I}}\boldsymbol{\psi}_r}{\boldsymbol{\psi}_r^T\boldsymbol{K}_{\mathrm{R}}\boldsymbol{\psi}_r} \tag{11}$$

In the proposed formulation (11) the modeshapes $\boldsymbol{\psi}_r$ are based on the undamped system and therefore real-valued. The used modeshapes are mass normalized and are determined by leaving out $\boldsymbol{K}_{\mathrm{I}}$ from the eigenvalue problem in equation (7)

$$\left(-\lambda^2\boldsymbol{M} + \boldsymbol{K}_{\mathrm{R}}\right)\boldsymbol{\psi} = \boldsymbol{0} \tag{12}$$

The symbol $\bar{\gamma}$ indicates the loss factors based on the undamped eigenmodes $\boldsymbol{\psi}$. Applying the undamped eigenmodes introduces an approximation in the calculation of the structural loss factors. The imaginary components introduced by the viscoelastic material are neglected. A revised formulation has been proposed by Xu et al. (2002) to provide a better approximation of the loss factor for high material loss factors. However, the revision is still limited to the undamped eigenmodes. Therefore, we propose to perform the structural loss factor calculation using the complex-valued modeshapes $\boldsymbol{\phi}$ from the complex-valued eigenvalue problem from equation (7). Then, the structural loss factor is given as

$$\gamma_r = \frac{\boldsymbol{\phi}_r^{\mathrm{H}}\boldsymbol{K}_{\mathrm{I}}\boldsymbol{\phi}_r}{\boldsymbol{\phi}_r^{\mathrm{H}}\boldsymbol{K}_{\mathrm{R}}\boldsymbol{\phi}_r} \tag{13}$$

To compare the performance of both formulations, equations (11) and (13), the obtained structural loss factors are compared to the Q-factor of the system. The structural loss factor and Q-factor are related via the used equivalence

$$\gamma_r = Q_r^{-1} \tag{14}$$

The Q-factor is determined based on the frequency response of the structure. The frequency response is

obtained by performing harmonic response analysis in the analyzed frequency range. The 3 dB method is applied to extract the Q-factor from the frequency response by dividing the resonant frequency by the half-power bandwidth, as described by Bert (1973). A constrained viscoelastic layer is used as example. Here, aluminum is applied as structural material with Young's modulus 70 GPa, density $2.7 \times 10^3\,\mathrm{kg/m^3}$ and Poisson ratio $\nu = 0.3$ and for the viscoelastic material: Young's modulus 1 GPa, density $1 \times 10^3\,\mathrm{kg/m^3}$ and Poisson ratio $\nu = 0.3$. The analyzed beam has a length of 2.25 m, a height of 0.15 m and unit thickness. Figure 1 illustrates the structure. The viscoelastic layer is centered along the beam with a total height of 0.05 m. The structure illustrates a rather extreme scenario in which the viscoelastic material has significant contribution to the deformation. For the first two eigenmodes both structural loss factors and Q-factor are determined. Furthermore, the comparison is performed for different values of the material loss factor η. The results are summarized in Table 1. The relative difference between the Q-factor and the structure's loss factor is significantly reduced by application of the complex-valued modeshapes $\boldsymbol{\phi}$. This reduction is mainly applicable for designs in which viscoelastic materials with high material loss factors are used and where large parts of the viscoelastic material are subjected to deformation for the analyzed modeshapes.

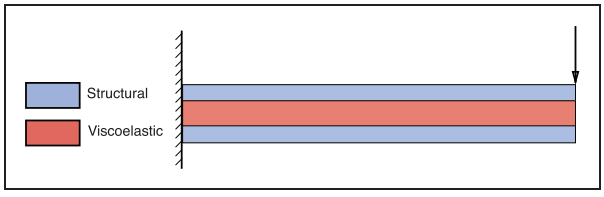

Figure 1. Illustration of the clamped cantilever beam containing a constrained viscoelastic layer. The arrow indicates the location of the excitation force and position measurement during dynamic loading.

3. Topology optimization of viscoelastic and structural material

The simultaneous distribution of both viscoelastic and structural material is realized using a multi-material topology optimization routine. The optimization method is mainly based on the study regarding multi-material, parametric optimization routines by Wang et al. (2015) and is briefly outlined here. We have opted for a level-set based approach, in order to obtain clearly distinct material regions. Trials using density-based multi-material topology optimization often resulted in designs containing mixtures of materials that are difficult to interpret.

3.1. Multi-material boundary representation

The level set method was originally developed by Osher and Sethian (1988) for the numerical computation of front and boundary propagation and has been applied in the context for shape optimization by Allaire et al. (2004) and Wang et al. (2003). In level set-based optimization routines the structural boundary is represented by the zero level set of an auxiliary scalar function, the so-called Level Set Function (LSF). Multi-material structures require multiple level set functions to describe the required material boundaries. Each level set defines the subdomains

$$\begin{cases} \varphi^k(\boldsymbol{X}) > 0, & \forall(\boldsymbol{X}) \in \Omega^k \backslash \Gamma^k \quad \text{(material)} \\ \varphi^k(\boldsymbol{X}) = 0, & \forall(\boldsymbol{X}) \in \Gamma^k \quad \text{(interface)} \\ \varphi^k(\boldsymbol{X}) < 0, & \forall(\boldsymbol{X}) \in D \backslash \overline{\Omega^k} \quad \text{(void)} \end{cases} \tag{15}$$

Table 1. Comparison between the structural loss factors and Q-factor of a structure containing a constrained viscoelastic layer (Figure 1). The loss factors $\bar{\gamma}$ and γ are determined using the undamped and damped eigenmodes. The relative difference is calculated between the structural loss factors and the inverse of the Q-factor to illustrating the improved prediction of damping behavior when using the complex-valued eigenmodes for the loss factor calculation.

η	Mode	Q^{-1}	$\bar{\gamma}_r$	Relative difference	γ_r	Relative difference
1.00	1	0.079	0.139	0.774	0.079	0.001
	2	0.289	0.416	0.434	0.307	0.059
0.75	1	0.072	0.105	0.448	0.073	0.007
	2	0.249	0.312	0.249	0.259	0.040
0.50	1	0.057	0.069	0.204	0.058	0.007
	2	0.187	0.208	0.114	0.191	0.021
0.25	1	0.034	0.035	0.025	0.033	0.011
	2	0.101	0.104	0.025	0.102	0.003

Here $\boldsymbol{X}$ is a point within the design domain, the index k indicates the use of k level set functions and D corresponds to the design domain. Two level set functions are required to describe two materials and void. The first level set function separates material from void, while the second level set function distinguishes the domains of viscoelastic and structural material. Figure 2 illustrates a material distribution using two level set functions. Using the formulation proposed earlier for elastic materials (Wang et al., 2015), we can now define the following stiffness and mass matrices for the considered structural and viscoelastic design problem

$$\begin{aligned} \boldsymbol{K}(\varphi) &= H(\varphi^1)\{(1 - H(\varphi^2))\boldsymbol{K}_{\mathrm{e}}^1 + H(\varphi^2)\boldsymbol{K}_{\mathrm{e}}^2\} \\ \boldsymbol{M}(\varphi) &= H(\varphi^1)\{(1 - H(\varphi^2))\boldsymbol{M}_{\mathrm{e}}^1 + H(\varphi^2)\boldsymbol{M}_{\mathrm{e}}^2\} \end{aligned} \tag{16}$$

Here $H(\varphi^k)$ represents the Heaviside function of the kth level set function, K_{e}^k and M_{e}^k correspond respectively to the elementary stiffness and mass matrices of material k. The applied Heaviside function is both approximated and regularized, as discussed in more detail in Section 3.5.

3.2. Parametric level set method

The topology optimization is implemented by a parametric level set method. In parametric methods a parameterization is applied to uncouple the space and time dependencies within the level set method (Luo et al., 2007; Wang and Wang, 2006). The level set functions are constructed by the summation of basis functions

$$\varphi^k(\boldsymbol{X}, t) = \sum_{i=1}^{N} \xi_i(\boldsymbol{X})\alpha_i^k(t) \tag{17}$$

Here N equals the total number of shape functions included in the design domain. The shape functions are given as $\xi_i(\boldsymbol{X})$, which describe the ith shape function. The expansion coefficients $\alpha_i^k(t)$ are applied to scale the individual shape functions. The variable t represents a pseudo-time variable and indicates the change of expansion coefficients throughout the iterations. The decoupling of the space and time dependencies allows us to apply gradient-based optimization routines, rather than solve Hamilton–Jacobi convection equations to update the structure's boundary. Besides, the parametric level set method allows to nucleate holes throughout the design domain by allowing negative values of the expansion coefficients (Luo et al., 2007). Different approaches are available to parameterize the level set function and to describe the level set functions (Van Dijk et al., 2013). In this study we apply a Compactly-Supported Radial Basis Function (CS-RBF) proposed by Wendland (1995) for the parameterization. These shape functions also have been applied in earlier parametric level set studies (Luo et al., 2008; Wang et al., 2015). The shape function is given as

$$\xi_i(\boldsymbol{X}) = \begin{cases} 0 & \text{if } r_i(\boldsymbol{X}) \geq 1 \\ ((1 - r_i(\boldsymbol{X}))^4(4r_i(\boldsymbol{X}) + 1) & \text{if } r_i(\boldsymbol{X}) < 1 \end{cases} \tag{18}$$

The radius r_i is given as

$$r_i(\boldsymbol{X}) = \frac{||\boldsymbol{X} - \boldsymbol{X}_i||}{R} \tag{19}$$

where R refers to the influence radius of the basis function. Only the neighboring elements within the influence radius will contribute to the function value of the level set function.

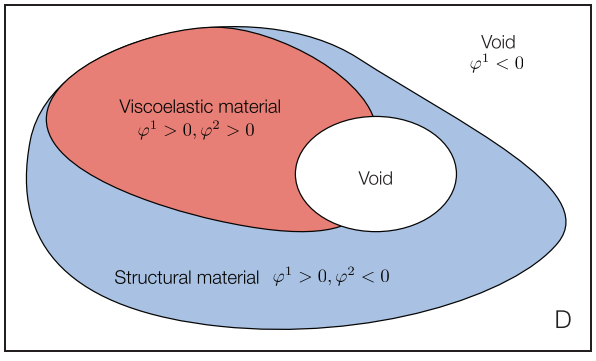

Figure 2. Illustration of a multi-material structure defined by two level set functions. The first level set function φ^1 determines the placement of material, while the second level set function φ^2 distinguishes between structural and viscoelastic material.

3.3. Optimization problem for structural loss factor maximization

In the parametric level set method the shape of the level set function is completely determined by the given expansion coefficients. By changing the values of the expansion coefficients local shape changes are realized. Therefore, the expansion coefficients are used as design variables during the optimization. The optimization problem is formulated as

$$\begin{aligned} \text{find} \quad & \alpha_i^k, \quad i = 1, 2, \ldots, N, \quad k = 1, 2 \\ \max \quad & J = \sum_r \gamma_r = \sum_r \frac{\phi_r^{\mathrm{H}} \boldsymbol{K}_{\mathrm{I}} \phi_r}{\phi_r^{\mathrm{H}} \boldsymbol{K}_{\mathrm{R}} \phi_r} \\ \text{s.t.} \quad & (\boldsymbol{K}' + i\boldsymbol{K}'')\phi = \lambda^2 \boldsymbol{M}\phi \\ & \phi_j^{\mathrm{H}} \boldsymbol{M} \phi_l = \delta_{jl} \\ & \Re(\lambda_1^2) \geq \Re({\lambda_{min}}^2) \end{aligned}$$

$$V^k \leq V^k_{\max}$$
$$\alpha^k_{i,\min} \leq \alpha^k_i \leq \alpha^k_{i,\max} \tag{20}$$

The optimization routine searches for the combination of expansion coefficients α^k_i to maximize the summation of the first r loss factors. In the presented work all loss factors have equal weight, however, it is also possible to define different weight factors for each modeshape. The optimization is subjected to the eigenvalue problem. The δ represents the Kronecker delta, furthermore, a minimum eigenfrequency of the structure is required to prevent development of low-frequency localized modes in viscoelastic material regions. Additionally, constraints can be added for the volume of either structural or viscoelastic material V^k. Finally, the design freedom of the optimizer is limited by specifying a lower $\alpha^k_{i,\min}$ and upper $\alpha^k_{i,\max}$ bound for the design variables.

3.4. Adjoint sensitivity analysis

An adjoint sensitivity analysis is performed to derive an exact formulation of the loss factor sensitivities. In this analysis we assume that all modes are of multiplicity one. The adjoint sensitivity analysis for discretized systems is discussed by Adelman and Haftka (1991) and is applied in the context of multi-material level set methods by Allaire et al. (2014). The formulation of the adjoint problem including a complex-valued eigenvalue problem is based on the adjoint sensitivity analysis given in Van der Veen et al. (2014). A similar approach is applied to add the adjoint variables $\boldsymbol{\mu}_1$ and μ_2 to the loss factor

$$\gamma^\star_r = \frac{\boldsymbol{\phi}^{\mathrm{H}}_r \boldsymbol{K}_{\mathrm{I}} \boldsymbol{\phi}_r}{\boldsymbol{\phi}^{\mathrm{H}}_r \boldsymbol{K}_{\mathrm{R}} \boldsymbol{\phi}_r} + \Re\left(\boldsymbol{\mu}^{\mathrm{H}}_1 \left(\boldsymbol{K} - \lambda^2_r M\right)\boldsymbol{\phi}\right) + \mu_2\left(\boldsymbol{\phi}^{\mathrm{H}} M \boldsymbol{\phi} - 1\right) \tag{21}$$

Taking the gradients with respect to the design variables α^k_i results in equation (22)

$$\frac{\partial \gamma^\star_r}{\partial \alpha^k_i} = \frac{\left\{ \begin{array}{l} \left(\phi^{\mathrm{H}}_r K_{\mathrm{R}} \phi_r\right)\left(2\phi^{\mathrm{H}}_r K_{\mathrm{I}} \frac{\partial \phi_r}{\partial \alpha^k_i} + \phi^{\mathrm{H}}_r \frac{\partial K_{\mathrm{I}}}{\partial \alpha^k_i}\phi_r\right) \\ -\left(\phi^{\mathrm{H}}_r K_{\mathrm{I}} \phi_r\right)\left(2\phi^{\mathrm{H}}_r K_{\mathrm{R}} \frac{\partial \phi_r}{\partial \alpha^k_i} + \phi^{\mathrm{H}}_r \frac{\partial K_{\mathrm{R}}}{\partial \alpha^k_i}\phi_r\right) \end{array} \right\}}{\left(\phi^{\mathrm{H}}_r K_{\mathrm{R}} \phi_r\right)^2}$$
$$+ \Re\left(\mu^{\mathrm{H}}_1 \left(\frac{\partial K}{\partial \alpha^k_i} - \lambda^2_r \frac{\partial M}{\partial \alpha^k_i} - \frac{\partial \lambda^2_r}{\partial \alpha^k_i} M \right)\phi_r \right.$$
$$+ \mu^{\mathrm{H}}_1 \left(K - \lambda^2_r M\right)\frac{\partial \phi_r}{\partial \alpha^k_i}\Bigg)$$
$$+ \mu_2\left(2\phi^{\mathrm{H}}_r M \frac{\partial \phi_r}{\partial \alpha^k_i} + \phi^{\mathrm{H}}_r \frac{\partial M}{\partial \alpha^k_i}\phi_r\right) \tag{22}$$

$$\frac{\partial \gamma^\star_r}{\partial \alpha^k_i} = \frac{\left(\phi^H_r K_{\mathrm{R}} \phi_r\right)\left(\phi^H_r \frac{\partial K_{\mathrm{I}}}{\partial \alpha^k_i}\phi_r\right) - \left(\phi^H_r K_{\mathrm{I}} \phi_r\right)\left(\phi^H_r \frac{\partial K_{\mathrm{R}}}{\partial \alpha^k_i}\phi_r\right)}{\left(\phi^H_r K_{\mathrm{R}} \phi_r\right)^2}$$
$$+ \Re\left(\mu^H_1\left(\frac{\partial K}{\partial \alpha^k_i} - \lambda^2_r \frac{\partial M}{\partial \alpha^k_i}\right)\phi_r\right) + \mu_2 \phi^H_r \frac{\partial M}{\partial \alpha^k_i}\phi_r \tag{23}$$

The adjoint multipliers $\boldsymbol{\mu}_1$ and μ_2 are chosen such that the modeshape sensitivities $\frac{\partial \phi_r}{\partial \alpha^k_i}$ and eigenfrequency sensitivities $\frac{\partial \lambda^2_r}{\partial \alpha^k_i}$ are not required to be calculated. The following adjoint problem has to be solved to determine the adjoint variables

$$\begin{bmatrix} \left(K - \lambda^2_r M\right) & 2M\phi_r \\ 2\phi^{\mathrm{H}}_r M & 0 \end{bmatrix}\begin{bmatrix} \boldsymbol{\mu}_1 \\ \mu_2 \end{bmatrix} = \begin{bmatrix} \frac{-\left(\phi^{\mathrm{H}}_r K_{\mathrm{R}} \phi_r\right)(2K_{\mathrm{I}}\phi_r) + \left(\phi^{\mathrm{H}}_r K_{\mathrm{I}} \phi_r\right)(2K_{\mathrm{R}}\phi_r)}{\left(\phi^{\mathrm{H}}_r K_{\mathrm{R}} \phi_r\right)^2} \\ 0 \end{bmatrix} \tag{24}$$

When the adjoint variables are known, the loss factor sensitivities are determined from the remaining terms in equation (22), as given in equation (23). To determine the loss factor sensitivity with respect to all design variables α^k_i requires to solve the adjoint problem (24) once per iteration for each considered mode. Then, equation (23) is solved for each design variable. The required sensitivities with respect to the stiffness and mass matrices can be derived from equations (16) and (17).

3.5. Numerical implementation

For the numerical implementation of the presented method, the design domain is discretized in four-node quadrilateral (Q4), square plane stress finite elements. The ersatz material model is applied to scale the material properties around the level set boundaries. This formulation is applied for its simplicity, but note that mixed materials can still appear in the domain near boundaries between material regions. This local effect can be reduced by mesh refinement by reducing the minimal size of the transition region between material regions. The Heaviside function and its derivative are implemented with the approximations (Wang et al., 2003)

$$H(\varphi^k) = \begin{cases} a, & \varphi^k \leq -\Delta \\ \frac{3(1-a)}{4}\left(\frac{\varphi^k}{\Delta} - \frac{(\varphi^k)^3}{3\Delta^3}\right) + \frac{1+\alpha}{2}, & -\Delta < \varphi^k < \Delta \\ 1, & \varphi^k \geq \Delta \end{cases}$$
$$\frac{\partial H}{\partial \varphi^k} = \begin{cases} \frac{3(1-a)}{4\Delta}\left(1 - \left(\frac{\varphi^k}{\Delta}\right)^2\right), & |\varphi^k| \leq \Delta \\ b, & |\varphi^k| > \Delta \end{cases} \tag{25}$$

This implementation of the smooth Heaviside can introduce some mixed regions within the domain. However, it has been observed that the problem has a tendency to result in clearly separated material regions. In the following numerical examples, the parameters are implemented as: $a = 0.001$, $b = 0.0005$, $\Delta = 1$, $\alpha^k_{i,\min} = -2$, $\alpha^k_{i,\max} = 2$. The parameter b is kept to a nonzero value to allow possible design changes after a point in the design has exceeded Δ. Otherwise, the sensitivity information equals zero and the design cannot be changed once the absolute value of the LSF has exceeded Δ. For each element in the discretization a shape function is introduced. Hence, the centers of the shape functions are aligned with the centers of the elements in mesh. The influence radius R is kept between two and four times the mesh size. The optimization problem is solved using the Method of Moving Asymptotes (MMA) as given in Svanberg (1987). This method iteratively solves nonlinear programming problems and is suited for general and structural optimization problems. In each step of the iterative process a strictly convex approximating subproblem is generated and solved. The resulting topologies are visualized based on the level set functions.

4. Numerical examples

This section presents a number of case studies to study the optimal design of damped structures for maximum dissipation, and to illustrate the performance of the proposed optimization routine. First, a cantilever beam is optimized. Secondly, a comparison is made between the application of different complex material moduli and their influence on the final designs. Finally, the optimization routine is applied to an existing structure with a limited design space.

4.1. Case study I: Cantilever beam

The design domain of the cantilever beam is given in Figure 3. The complete cantilever beam is provided as design domain for the optimization. The cantilever is fixed on the left side, the remaining boundaries are unconstrained. The domain is discretized with $L = 70$ and $H = 20$ elements. The first level set function describes the structural material. For the structural material steel is applied with Young's modulus $E_1 = 200\,\text{GPa}$, Poisson ratio $\nu_1 = 0.3$ and density $\rho_1 = 7.85 \times 10^3\,\text{kg/m}^3$. Any damping introduced by the structural material is neglected, as this is much smaller than the damping provided by the viscoelastic material. The second level set function models the viscoelastic material and general material properties are applied to model the viscoelastic behavior with Young's modulus $E_2 = 1\,\text{GPa}$, Poisson ratio $\nu_2 = 0.3$ and density $\rho_2 = 1.0 \times 10^3\,\text{kg/m}^3$. A complex shear

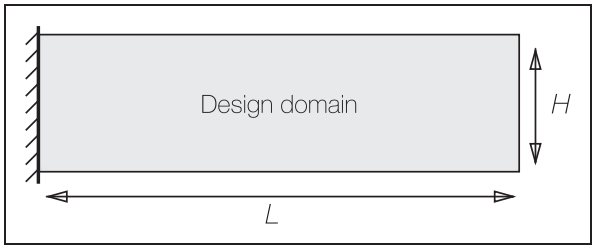

Figure 3. The design domain for case study I.

modulus with a material loss factor of $\eta_{\text{shear}} = 1.0$ is applied to model the dissipative properties. The value of the shear modulus is derived from the Young's modulus and Poisson ratio as

$$G = \frac{E}{2(1+\nu)} \tag{26}$$

The optimization is initialized with two constant level set functions. The initial values are chosen slightly above the zero level set, such that the design is initially filled with material which is a mixture of structural material with a small amount of viscoelastic material available. Since the level set functions are initialized as constant values above the zero level set, the design domain is completely filled by elements with scaled material properties with respect to the values of both initial LSFs. The objective of the optimization is to maximize the average of the structural loss factors corresponding to the first two eigenmodes. This represents a simplified form of optimizing the dissipation within a certain frequency band which contains both eigenfrequencies. The optimization is constrained such that only 40% of the design domain may be occupied by viscoelastic material. Furthermore, a frequency constraint is applied to keep the first eigenfrequency within 50% of the eigenfrequency of the initial design. We mainly apply the frequency constraint to prevent the creation of low-frequency internal modes in the viscoelastic material regions with high structural loss factors. Therefore, the chosen percentage can be chosen to match any practical frequency requirements.

The optimization is terminated when all constraints are satisfied and when the final objective value is within 1% of the previous three objective values. Figure 4 shows the progression of the design throughout the iterations, with the final design given in Figure 4d. The general layout of the viscoelastic material resembles a constrained-layer damping configuration, as the viscoelastic material is mainly distributed along the centerline of the cantilever. After 35 iterations the final design achieved an objective value of $J = 0.5075$. The result can be compared with a cantilever with the same aspect ratio with a conventional constrained layer damping configuration, which provides

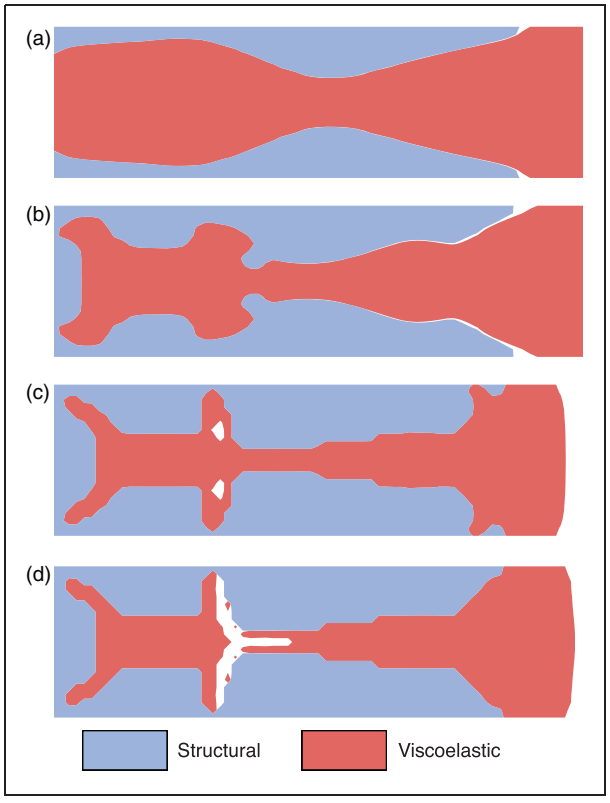

Figure 4. The design progression throughout the optimization routine at iteration 2, 5, 20 and 35 and the corresponding objective values. (a) Iteration 2, $J = 0.1651$, (b) Iteration 5, $J = 0.3761$, (c) Iteration 20, $J = 0.4553$, and (d) Iteration 35, $J = 0.5075$.

a structural loss factor between roughly 0.26 and 0.39 for a centered, viscoelastic layer between respectively three and seven elements. The optimized design is able to achieve higher structural loss factors compared to the conventional configurations.

The history of the objective values and the corresponding loss factors of the two modeshapes are given in Figure 5. Similarly, Figure 6 presents the progression of the volume and frequency constraints. The constraint values are normalized with respect to the maximum value of the constraint. For this formulation positive values represent unsatisfied constraints, while negative values correspond to satisfied constraints. All constraints remain satisfied at the end of the optimization.

The application of the complex shear modulus results only in energy dissipation when the viscoelastic material is subjected to shear deformation. Therefore, the performance of the obtained designs can be visualized by plotting the shear deformation of each element. The maximum in-plane shear strain is determined as

$$\varepsilon_{\max} = \sqrt{\left(\frac{\varepsilon_x - \varepsilon_y}{2}\right)^2 + \varepsilon_{xy}^2} \tag{27}$$

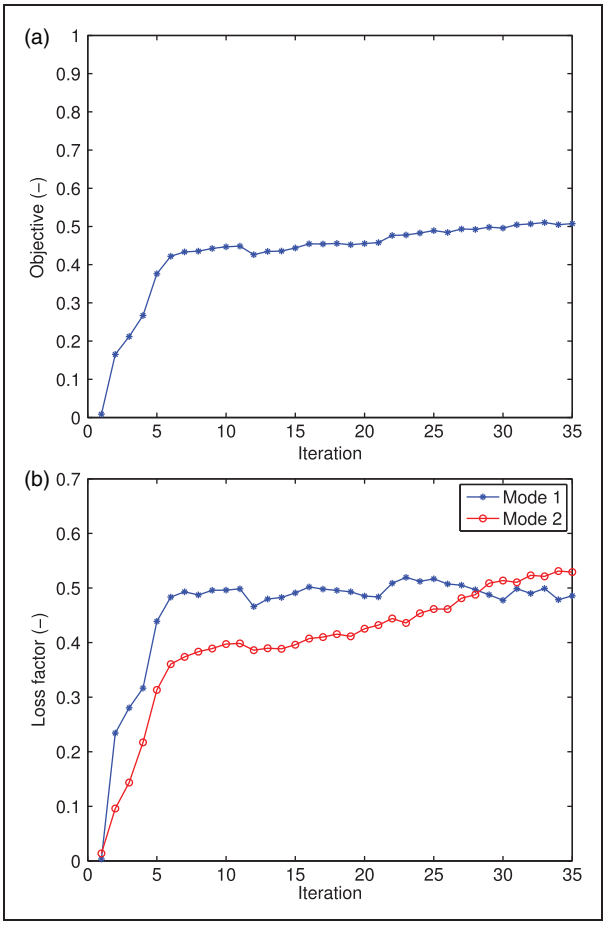

Figure 5. The history of the objective values (a) and corresponding loss factors (b) during the optimization.

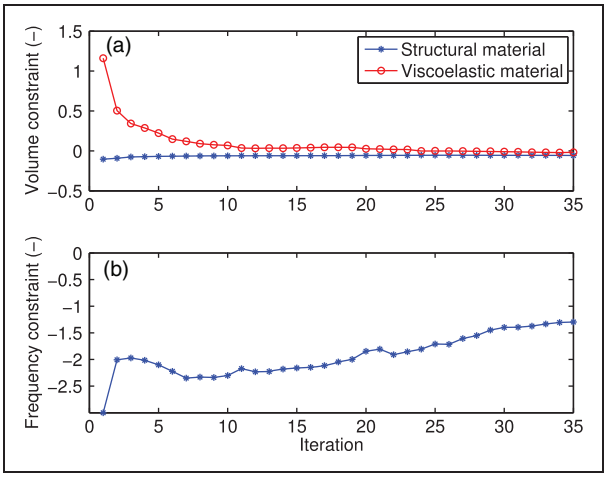

Figure 6. The history of the volume (top) and frequency (bottom) constraint values during the optimization. The constraints are normalized with respect to the specified maximum value. Positive values represent unsatisfied constraints.

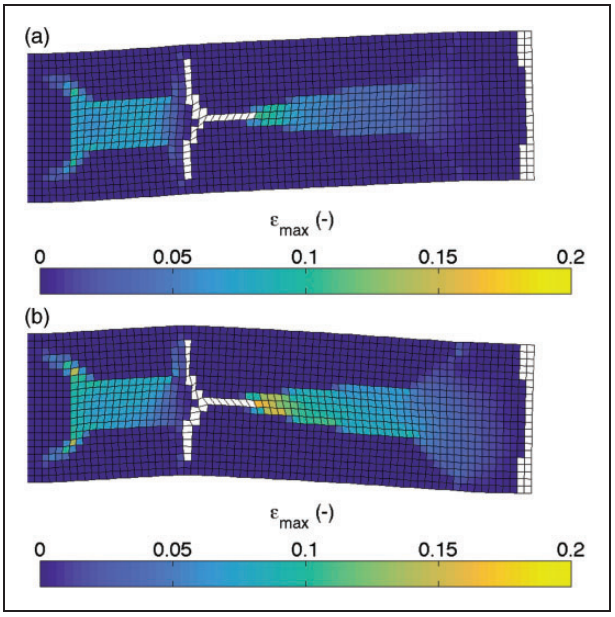

Figure 7. The deformation shapes and corresponding maximum shear strain ε_{max} for the first (a) and second (b) eigenmode of the optimized structure. The uncolored elements represent void elements within the design.

To compare the deformation between both modeshapes a base excitation is applied. The eigenmodes of the structure only provide information on the deformation shape and not on the actual amplitude of the deformation. Therefore, the first and second eigenmodes are excited with the same harmonic acceleration profile at the clamped side of the cantilever. Figure 7 shows the resulting deformation shapes and the maximum shear strain. The shear strain is mostly visible in the viscoelastic material. In both eigenmodes the viscoelastic material is effectively used, as almost all viscoelastic elements are subjected to shear strain. In the second mode, slightly higher strain values are observed, corresponding to the slightly higher structural loss factor of the second modeshape. Figure 8 illustrates a contour plot of the energy dissipated per element for the first modeshape of the structure. The obtained energy is directly related to the shear deformation observed for this modeshape, as illustrated in Figure 7a. The dissipated energy is calculated by equation (10) and is normalized with respect to the element with highest dissipation. The direct relation between shear deformation and dissipated energy is observed when comparing the figures of shear strain and dissipated energy (Figures 7a and 8).

4.2. Design influences by complex moduli

In the previous case study the viscoelastic material has been described with a complex shear modulus.

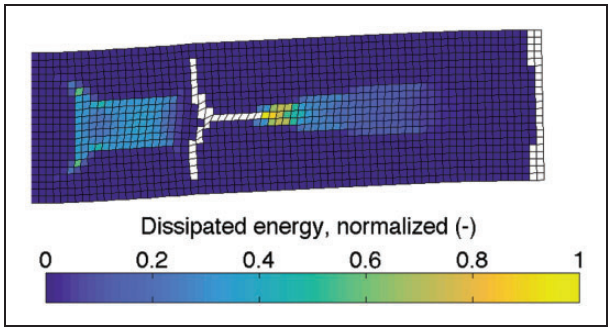

Figure 8. The energy dissipated for each element for the first eigenmode of the structure. The values are normalized with respect to the maximum energy dissipated in an element. The obtained result is directly related to the shear strain given in Figure 7a. The uncolored represent void elements within the design.

However, as discussed in Section 2 the viscoelastic material can also be represented with either a complex Young's or complex bulk modulus. To illustrate the influence of the different modeling approaches, the optimization of case I will be evaluated separately for a complex shear, Young's and bulk modulus. For each complex modulus a corresponding material loss factor of $\eta = 1$ is applied. The remaining material parameters and the design space are kept the same. However, in this optimization only the structural loss factor corresponding to the first eigenmode is considered as the objective. The optimizations were terminated after the objective value converged and all constraints were satisfied. The optimization with a shear, Young's and bulk modulus provide the objective values: $J_G = 0.6002$, $J_E = 0.8823$, $J_\kappa = 0.6940$. The obtained designs are given in Figure 9. The material layout of the three designs show significant differences. For the complex shear modulus the material is mainly located in the center of the design, similar to conventional constrained layer configurations. For the complex bulk modulus, the material is mainly located at the outer edge of the domain, where the normal strains are the highest. In the design using a complex Young's modulus, the viscoelastic material is mainly located at the right side of the cantilever, where it is subjected to both normal and shear strains. The performance of the designs are illustrated by plotting the in-plane maximum shear strains, equation (27), as well as the maximum in-plane principal strains within the structure

$$\varepsilon_{1,2} = \frac{\varepsilon_x + \varepsilon_y}{2} \pm \sqrt{\left(\frac{\varepsilon_x - \varepsilon_y}{2}\right)^2 + \varepsilon_{xy}^2} \tag{28}$$

The design based on a complex shear modulus shows almost identical principal strains as maximum shear strains, illustrating that most of the viscoelastic material is subjected to shear deformation. On the other hand, the design using the complex bulk modulus

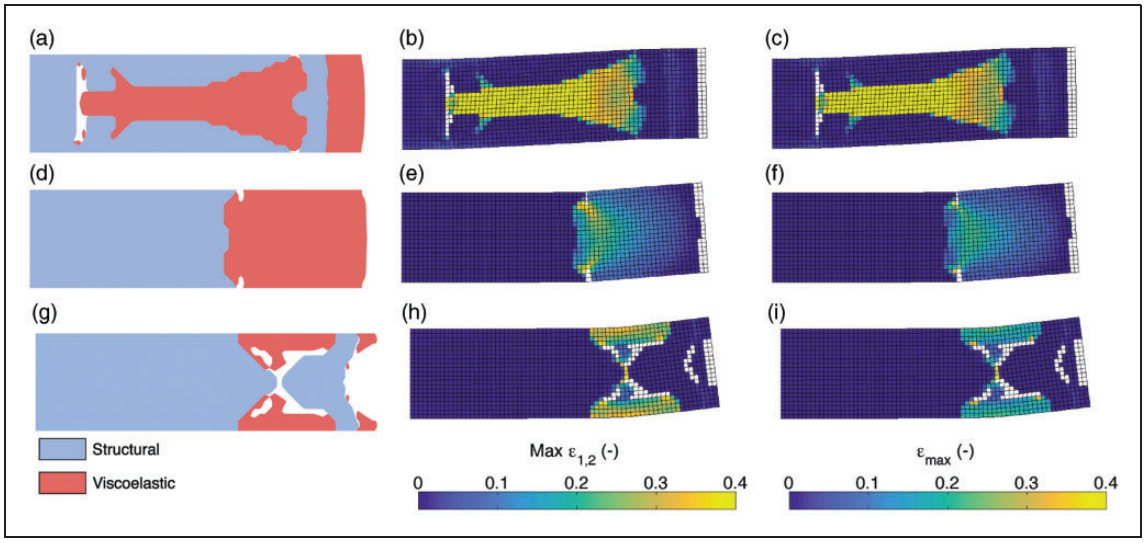

Figure 9. A comparison between the optimized designs and their performance for the application of multiple complex material models: (a): shear, (d): Young's and (g): bulk modulus. The differences in performance are highlighted by the maximum principal and maximum shear strains within the structure for the first eigenmode. (a) Complex shear modulus, J_G = 0.6002, (b) Max principal strain, (c) Max shear strain, (d) Complex Young's modulus, J_E = 0.8823, (e) Max principal strain, (f) Max shear strain, (g) Complex bulk modulus, J_κ = 0.6940, (h) Max principal strain and (i) Max shear strain.

shows higher maximum principal strains, illustrating that the viscoelastic material is mainly subjected to normal strains. The complex Young's modulus contains a combination of both shear and normal deformations. The higher loss factor achieved by the complex Young's modulus is understood, since any deformation of the viscoelastic material will result in energy dissipation for the complex Young's modulus, while in the complex shear and bulk modulus only the shear or normal strain components dissipate energy.

4.2.1. Performance cross-check. To illustrate that the obtained designs only show optimized performance for the material model used during the optimization, an additional verification is performed. The structural loss factor for each optimized design is evaluated with the other two complex material models. This is to show the impact of the used material model on the optimization process. This is done for all combinations of material moduli and results are given in Table 2. Since the complex Young's modulus dissipates energy for any deformation, it is observed that all designs evaluated with this modulus provide reasonable or even improved performance. However, a significant performance difference is observed between the complex shear and bulk modulus.

Table 2. A comparison between the loss factors for the optimized designs, when the performance is evaluated with different material models than used during the optimization.

	Modulus for performance check		
Modulus during optimization	*G*	*E*	κ
G	0.6002	0.6298	0.0341
E	0.1838	0.8823	0.4834
κ	0.0206	0.7168	0.6940

4.3. Case study II: Existing structure with limited design domain

The second case study illustrates the ability to generate a design to damp a particular mode of an existing structure. In this case study a clamped beam is studied as existing structure. The beam is clamped at both sides and cannot be modified by the optimization. A limited design domain is defined on top of the cantilever. The optimization routine is only allowed to develop designs within this domain. An illustration of the design and nondesign domains are given in Figure 10. The objective of the optimization is to achieve maximum loss factor for the first eigenmode of the structure. The material properties are the same as applied in Section 4.1 and a complex shear modulus with a material loss factor of $\eta_{\text{shear}} = 1$ is applied for the viscoelastic material.

The optimization is subject to two constraints: the final design should utilize more than half of the total design domain and the volume fraction of the viscoelastic material is limited to half of the total design domain.

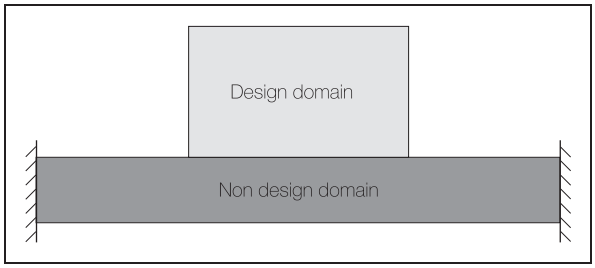

Figure 10. The design and nondesign domains for case study II. The nondesign domain is clamped at both sides and cannot be modified by the optimization routine.

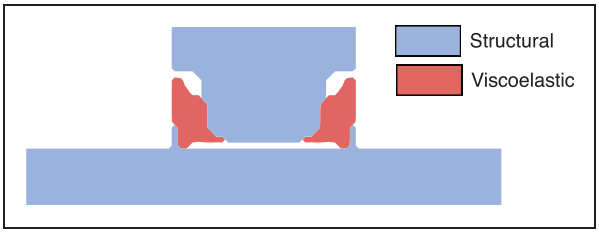

Figure 11. The final design of the optimization achieved after 58 iterations. The design achieved an objective value of $J = 0.3803$.

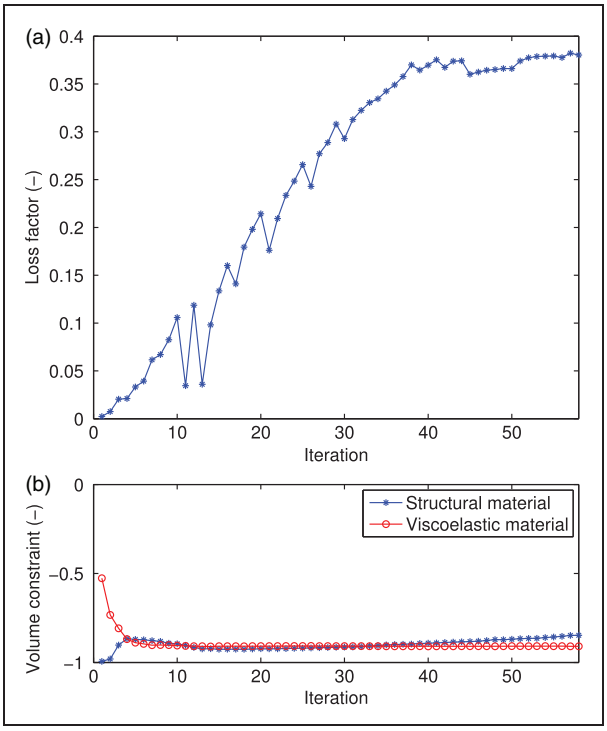

Figure 12. The history of the loss factor (a) and normalized volume and frequency constraints (b) during the optimization.

The frequency constraint is omitted in this optimization routine, since the existing structure prevents the creation of very low-frequency resonant modes.

The final design achieved after 58 iterations is given in Figure 11. The optimization results in $J = 0.3803$. Figure 12a presents the history of the loss factor and Figure 12b shows the history of the volume and frequency constraints. All applied constraints remain satisfied after 58 iterations.

The optimization has developed a design which resulted in a loss factor of 0.3803 for the first eigenmode. The performance of the design is illustrated by plotting the dissipated energy per element during oscillation in Figure 13. During the first eigenmode the structure within the design domain resonates in phase with the beam. The relative displacement of the top part is larger compared to the displacement of the beam, straining the viscoelastic material and dissipating energy during oscillation. The behavior of the generated design is similar to tuned mass damper systems and attenuates the first resonant mode of the structure.

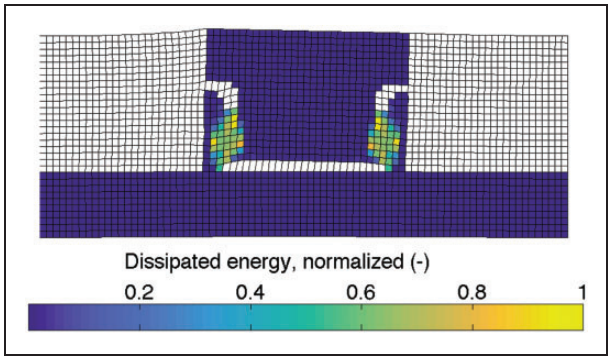

Figure 13. The deformation shape for the first eigenmode of the optimized structure of case study II. The dissipated energy in each element is plotted to illustrate the energy dissipation for the first eigenmode. The uncolored elements correspond to void elements in the design.

5. Discussion

A systematic design approach has been presented for the development of damped structures using a combination of viscoelastic and structural materials. The optimization routine has shown to be capable of generating structures with high loss factors and improving the damping of a given structure. While the presented method provides promising results, a number of difficulties and assumptions remain. The current method optimizes the structures for a specified eigenmode. However, by the introduction of structural and viscoelastic material the possibility exists to introduce new modeshapes at lower frequencies. Also, the change of the design might switch the order of modeshapes,

especially for designs where eigenfrequencies are close together. A mode tracking procedure could be added to the proposed method to handle such events. Moreover, when multiplicity of eigenvalues is encountered additional measures are required to determine the eigenmode sensitivities, since the eigenmodes can change discontinuously during a crossing of eigenvalues.

Moreover, the applied viscoelastic material model has a significant influence on the performance of the optimization routine. As illustrated in Section 4.2, the application of different complex moduli results in large differences between the optimized designs. Therefore, an accurate material model is required to describe the viscoelastic behavior. Of particular importance are its dissipative properties, as the optimization routine will exploit any dissipative behavior included in the material model.

Finally, the implemented viscoelastic material model contains two assumptions: both temperature and excitation frequency dependencies are neglected. This considerably simplifies the behavior of the viscoelastic material. However, depending on the applied viscoelastic material, both parameters can have significant influence on the dissipative properties of the material. To extend the model to capture the thermal behavior requires a separate thermal analysis to determine the steady state temperature during oscillation. If temperature peaks occur within the viscoelastic material, its dissipative properties are reduced, resulting in lower structural loss factors than predicted. This results in a fully coupled thermomechanical problem that must be solved iteratively. A workaround is to introduce additional thermal constraints within the optimization routine to keep the temperature of the viscoelastic material between specified boundaries. The coupling with thermal behavior is left as future work.

6. Conclusions

A well-performing topology optimization approach has been presented that can generate multi-material designs with optimized damping properties. The employed level-set based formulation yields a clear separation between various material phases. Structural loss factors using complex-valued eigenmodes have been found to provide an accurate assessment of damping characteristics, even for designs with high volume fractions of viscoelastic material combined with high material loss factors.

In various examples, we have demonstrated that designs were obtained achieving higher structural loss factors than conventional constrained layer configurations. Also, the optimization method is successfully applied to attenuate a resonant mode of an existing structure. The generated design shows behavior similar to tuned mass damper systems and adds significant damping to the resonant mode of interest. The method has the potential to be applied to complicated structures and can be extended towards three-dimensional designs. The influence of different viscoelastic material models is investigated and significantly different results are found. To achieve suitable designs, the chosen viscoelastic material has to adequately reflect the behavior of the actual material.

Declaration of Conflicting Interests

The author(s) declared no potential conflicts of interest with respect to the research, authorship, and/or publication of this article.

Funding

The author(s) received no financial support for the research, authorship, and/or publication of this article.

References

Adelman HM and Haftka RT (1991) A discourse on sensitivity analysis for discretely-modeled structures. Technical Report, NASA, USA, March.

Allaire G, Dapogny C, Delgado G, et al. (2014) Multi-phase structural optimization via a level set method. *ESAIM: Control, Optimization and Calculus of Variations* 20(2): 576–611.

Allaire G, Jouve F and Toader AM (2004) Structural optimization using sensitivity analysis and a level-set method. *Journal of Computational Physics* 194(1): 363–393.

Bert CW (1973) Material damping - An introductory review of mathematical models, measures and experimental techniques. *Journal of Sound and Vibration* 29(2): 129–153.

De Vreugd J, de Lange D, Winters J, et al. (2014) Damping in space constructions. *European Conference on Spacecraft Structures, Materials & Environmental Testing*. 1–4 April, Braunschweig, Germany: ESA

El-Sabbagh A and Baz A (2013) Topology optimization of unconstrained damping treatments for plates. *Engineering Optimization* 46(9): 1153–1168.

Gielesen W, de Bruijn D, van den Dool T, et al. (2013) *Gaia basic angle monitoring system. SPIE Optical Engineering+ Applications. International Society for Optics and Photonics*. 25 August 2013, San Diego, California, United States: International Society for Optics and Photonics.

Grootenhuis P (1970) The control of vibrations with viscoelastic materials. *Journal of Sound and Vibration* 11(4): 421–433.

Huang X and Xie YM (2009) Bi-directional evolutionary topology optimization of continuum structures with one or multiple materials. *Computational Mechanics* 43(3): 393–401.

Johnson CD (1995) Design of passive damping systems. *Journal of Vibration and Acoustics* 117(B): 171.

Johnson CD and Kienholz DA (1982) Finite element prediction of damping in structures with constrained viscoelastic layers. *AIAA Journal* 20(9): 1284–1290.

Kang Z, Zhang X, Jiang S, et al. (2012) On topology optimization of damping layer in shell structures under

harmonic excitations. *Structural and Multidisciplinary Optimization* 46(1): 51–67.

Kerwin EM (1959) Damping of flexural waves by a constrained viscoelastic layer. *The Journal of the Acoustical Society of America* 31(7): 952–962.

Kim SY (2011) *Topology design optimization for vibration reduction: Reducible design variable method*. PhD Thesis, Queen's University, Canada.

Ling Z, Ronglu X, Yi W, et al. (2011) Topology optimization of constrained layer damping on plates using method of moving asymptote (MMA) approach. *Shock and Vibration* 18(1–2): 221–244.

Liu ZX, Guan H and Zhen WG (2013) Topology optimization of viscoelastic materials distribution of damped sandwich plate composite. *Applied Mechanics and Materials* 347-350: 1182–1186.

Lumsdaine A and Scott RA (1998) Shape optimization of unconstrained viscoelastic layers using continuum finite elements. *Journal of Sound and Vibration* 216(1): 29–52.

Lunden R (1980) Optimum distribution of additive damping for vibrating frames. *Journal of Sound and Vibration* 72(3): 391–402.

Luo J, Luo Z, Chen L, et al. (2008) A semi-implicit level set method for structural shape and topology optimization. *Journal of Computational Physics* 227(11): 5561–5581.

Luo Z, Tong L, Wang MY, et al. (2007) Shape and topology optimization of compliant mechanisms using a parameterization level set method. *Journal of Computational Physics* 227(1): 680–705.

Osher S and Sethian J (1988) Front propagating with curvature dependent speed: Algorithms based on Hamilton–Jacobi formulations. *Journal of Computational Physics* 79: 12–49.

Plunkett R and Lee CT (1970) Length optimization for constrained viscoelastic layer damping. *The Journal of the Acoustical Society of America* 48(1): 150–161.

Rao DK (1978) Vibration damping of tapered unconstrained beams. *Acustica* 39: 264–269.

Rao MD (2003) Recent applications of viscoelastic damping for noise control in automobiles and commercial airplanes. *Journal of Sound and Vibration* 262(3): 457–474.

Rittweger A, Albus J, Hornung E, et al. (2002) Passive damping devices for aerospace structures. *Acta Astronautica* 50(10): 597–608.

Samali B and Kwok K (1995) Use of viscoelastic dampers in reducing wind- and earthquake-induced motion of building structures. *Engineering Structures* 17(9): 639–654.

Sigmund O (2001) Design of multiphysics actuators using topology optimization - Part II: Two-material structures. *Computer Methods in Applied Mechanics and Engineering* 190(49–50): 6605–6627.

Svanberg K (1987) The method of moving asymptotes - A new method for structural optimization. *Numerical Methods in Engineering* 24: 359–373.

Tabak E, Goeij BD, Riel LV, et al. (2013) Design, building and testing of a Sun calibration mechanism for the MSI-VNS instrument on Earthcare. *Conference proceedings of the 15th European Space Mechanisms & Tribology Symposium*. 25–27 September, Noordwijk, The Netherlands: ESA.

Tschoegl NW (1989) *The Phenomelogical Theory of Linear Viscoelastic Behavior*. Berlin: Springer-Verlag.

Van der Veen G, Langelaar M and van Keulen F (2014) Integrated topology and controller optimization of motion systems in the frequency domain. *Structural and Multidisciplinary Optimization* 51(3): 673–685.

Van Dijk NP, Maute K, Langelaar M, et al. (2013) Level-set methods for structural topology optimization: A review. *Structural and Multidisciplinary Optimization* 48(3): 437–472.

Wang BQ, Wang BL and Huang ZY (2014) Topology optimization for constrained layer damping plates using evolutionary structural optimization method. *Advanced Materials Research* 894: 158–162.

Wang MY and Wang X (2004) Color level sets: A multi-phase method for structural topology optimization with multiple materials. *Computer Methods in Applied Mechanics and Engineering* 193(6-8): 469–496.

Wang MY, Wang X and Guo D (2003) A level set method for structural topology optimization. *Computer Methods in Applied Mechanics and Engineering* 192(1–2): 227–246.

Wang R, Crocombe AD, Richardson G, et al. (2008) Energy dissipation in spacecraft structures incorporating bolted joints operating in macroslip. *Journal of Aerospace Engineering* 21(1): 19–26.

Wang S and Wang MY (2006) Radial basis functions and level set method for structural topology optimization. *International Journal for Numerical Methods in Engineering* 65(12): 2060–2090.

Wang Y, Luo Z, Kang Z, et al. (2015) A multi-material level set-based topology and shape optimization method. *Computer Methods in Applied Mechanics and Engineering* 283: 1570–1586.

Wang YJ, Yau JD and Wei QC (2013) Vibration suppression of train-induced multiple resonant responses of two span continuous bridges using VE dampers. *Journal of Marine Science and Technology* 21(2): 149–158.

Wendland H (1995) Piecewise polynomial, positive definite and compactly supported radial functions of minimal degree. *Advances in Computational Mathematics* 4(1): 389–396.

Xu Y, Liu Y and Wang B (2002) Revised modal strain energy method for finite element analysis of viscoelastic damping treated structures. *Proceedings of SPIE*. Vol 4697, 17 March, San Diego, CA, USA: International Society for Optics and Photonics, pp. 35–42.

Yin L and Ananthasuresh G (2001) Topology optimization of compliant mechanisms with multiple materials using a peak function material interpolation scheme. *Structural and Multidisciplinary Optimization* 23(1): 49–62.

Zheng H, Cai C and Tan XM (2004) Optimization of partial constrained layer damping treatment for vibrational energy minimization of vibrating beams. *Computers and Structures* 82: 2493–2507.

Zheng W, Lei Y, Li S, et al. (2013) Topology optimization of passive constrained layer damping with partial coverage on plate. *Shock and Vibration* 20(2): 199–211.